JOURNAL OF CATALYSIS 16, 281–291 (1970)

The Structure of Raney Nickel

II. Electron Microprobe Studies

J. FREEL, W. J. M. PIETERS, AND R. B. ANDERSON

Department of Chemical Engineering, McMaster University, Hamilton, Ontario

Received June 2, 1969

The activation of Raney nickel alloys containing 42 and 50 wt % Ni by reaction with aqueous sodium hydroxide was studied by metallographic methods including an electron probe microanalyzer. The alloys contained a eutectic of about 5 wt % Ni, $\beta(NiAl_3)$, and $\gamma(Ni_2Al_3)$ phases; NiAl was not found in these alloys. For any phase the attack by alkali advances as a front yielding a sharp gradient between alloy and activated catalyst, or, in the case of eutectic, a void. In activated catalysts portions originating from β and γ alloys can be recognized on the basis of structural characteristics. The activated materials contain what appears to be shrinkage cracks, which are larger and more numerous in catalyst derived from β- rather than γ-phase. In moderately concentrated aqueous alkali, the eutectic and β phase react more rapidly than γ phase. For example, in a 10-min leaching of 30–50 mesh alloy at 50°C in which half of the aluminum was oxidized, the product contained activated β-phase and γ alloy. In dilute alkali the attack on the alloy was nonselective and the catalyst contained substantial amounts of alumina. Our data indicate that analyses of moderate accuracy can be obtained on the porous activated Raney nickel by the electron probe microanalyzer.

INTRODUCTION

In the preparation (*1*) of Raney nickel, a large part of the aluminum is converted to sodium aluminate, most of which is removed in subsequent water washing. The starting Raney alloys normally contain 40 to 50 wt % nickel. Alloys of higher nickel content usually contain significant amounts of the compound NiAl, which does not react with alkali (*2*), while alloys containing less nickel yield correspondingly less catalyst. Alloys in the composition range of 40–50 wt % nickel are not homogeneous, but may contain several phases (*3*). The structure of the initial alloys and their reactivity toward alkali is therefore an interesting feature of the Raney catalyst.

Various authors have investigated aspects of this problem. Littman and Bliss (*4*) described optical micrographs of commercially extracted catalyst in which two distinct areas could be observed and suggested that these might be related to the phases present in the original alloy. Mason (*5*) demonstrated this retention of the alloy appearance more clearly. The effect of alloy structure on catalytic activity of the extracted catalyst has also been examined (*2, 5*). However, several anomalies still remain; for example, different authors have reported that $NiAl_3$ is (*2*) and is not (*6*) more reactive toward alkali than Ni_2Al_3.

In the present study, we used the techniques of optical metallography to examine the microstructure of commercial Raney alloys and their reaction with sodium hydroxide to form Raney nickel. The interpretation of optical appearance was greatly facilitated by the use of an electron probe microanalyzer. Apparently analytical data of moderate accuracy can be obtained for the porous catalysts.

EXPERIMENTAL METHODS

Two large batches of commercial Raney alloy, nominally of 42 and 50 wt % nickel

composition [alloys A and B of Part I (7)] were used throughout.

Standard metallographic procedures were used in mounting and polishing specimens. Raney alloys were mounted in bakelite. Fully and partly extracted catalysts were pyrophoric, and were stored in ethanol to prevent oxidation. These samples were placed in glass moulds together with ethanol. A liquid, cold-mounting resin was added when most of the ethanol had evaporated. Polishing appeared to inhibit atmospheric oxidation substantially. The prepared surface was stable for several hours in terms of optical appearance, after which discoloration and surface pitting could be observed. Samples allowed to oxidize vigorously in air prior to mounting had a uniform, strongly reflecting surface devoid of the optical features of the normal catalyst.

An "Acton" electron probe microanalyzer (fixed angle of takeoff = 18°) was used at a beam voltage of 25 kV and specimen current 50 nA unless otherwise stated. Quartz and mica diffraction crystals were used to obtain the nickel and aluminum $K\alpha_1$ lines, respectively.

Good conduction of electrons away from the probe impact area is essential to avoid overheating or "hot spot" formation. Specimens were found to be sufficiently conducting after vacuum deposition of a layer of carbon about 1000 Å thick.

Samples of several nickel–aluminum intermetallic compounds, kindly furnished by Professor G. R. Purdy of this University, were used in preparing calibration curves for nickel and aluminum, as given in Fig. 1. The standard alloys were prepared by repeated nonconsumable-electrode arc melting in argon. The samples were weighed before and after melting and the alloys were checked metallographically for homogeneity.

Results

1. *The Structure of Commercial Raney Alloys*

Possible phases for nickel–aluminum alloys containing 40–50 wt % nickel, taken from the phase diagram of Alexander and Vaughan (3), are given in Table 1. These phases have been designated in different ways, and we have used the symbols in Table 1, to remain consistent with the work of Mason (5), which is most pertinent to the present study. Eutectic, $NiAl_3$ and Ni_2Al_3 may be clearly distinguished in an unetched, polished surface of such alloys (see Fig. 3A). Etchants are required (3) to reveal the compound NiAl, but none was detected in the present study either by etchants or by electron probe microanalysis of γ-phase grains.

TABLE 1
Possible Phases for Nickel–Aluminum Alloys Containing 40–50 wt % Nickel

Phase	Symbol	Nickel content (wt %)
Solid solutions of Ni in Al(I)	α	0.05 or less
I + $NiAl_3$	Eutectic	~5
$NiAl_3$	β	42
Ni_2Al_3	γ	56–60
NiAl	δ	80–83

The 42 and 50 wt % nickel alloys, received as irregular chips about ¼ cm^3 in volume, were crushed mechanically and screened in U. S. Standard sieves. For both alloys, six mounts, each containing some thirty 30–50 mesh pieces, were examined optically. Volume concentrations of γ-, β-, and eutectic phases in the two alloys, calculated by standard metallographic methods (8), are given in Table 2. For each of the alloys the amounts of the phases varied moderately. Pieces of 50/50 alloy, for example, contained from 54 to 66 vol % γ, those of 42/58 from 25 to 50%. However, all pieces of the former examined contained little eutectic, all of the latter, substantial amounts. The aluminum-rich alloy (42/58) contained significantly less γ-phase than the (50/50) alloy.

TABLE 2
Phase Analysis of Raney Nickel Alloys

Sample alloy	γ (av vol %)	β (av vol %)	Eutectic (av vol %)
A 50/50	58	40	~
B 42/58	30	45	25

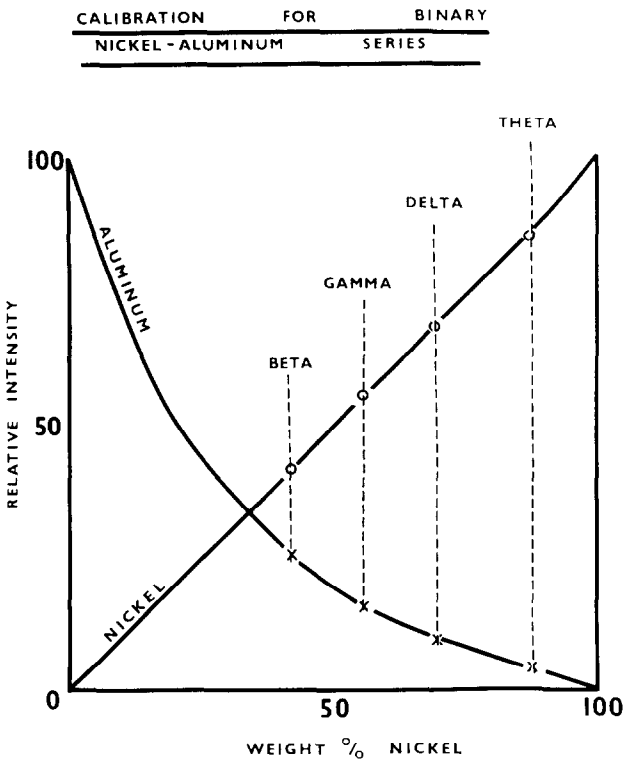

FIG. 1. Electron probe calibration for nickel–aluminum system at 25 kV.

Typical micrographs of 30–50 mesh pieces of the alloys are given in Figure 3B and C. As reported previously (*5*), γ-phase grains in 50/50 alloy were significantly larger than those in 42/58. The smaller grains of Ni_2Al_3 in the 42/58 alloy often showed typical dendritic structure.

The composition of these phases was confirmed by electron probe microanalysis. The aluminum-rich/nickel-deficient nature of the eutectic precipitate is illustrated in the probe scane shown in Fig. 4. Figure 4A is an oscilloscope display of the specimen current from a region containing β and eutectic only, the eutectic appearing as bright areas, and Figure 4B and C are records of the aluminum and nickel $K\alpha_1$ yields, respectively.

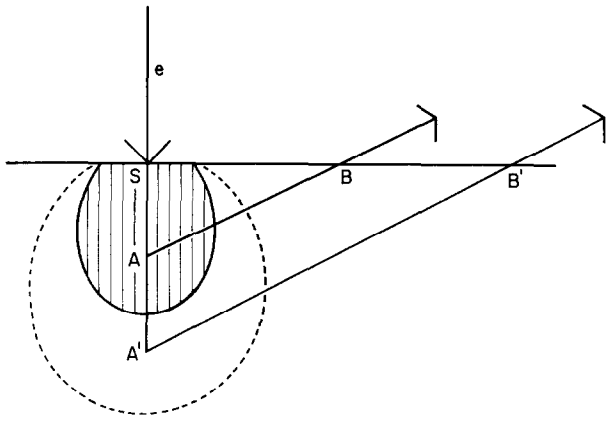

FIG. 2. Schematic representation of X-radiation in the same solid in microporous and nonporous form.

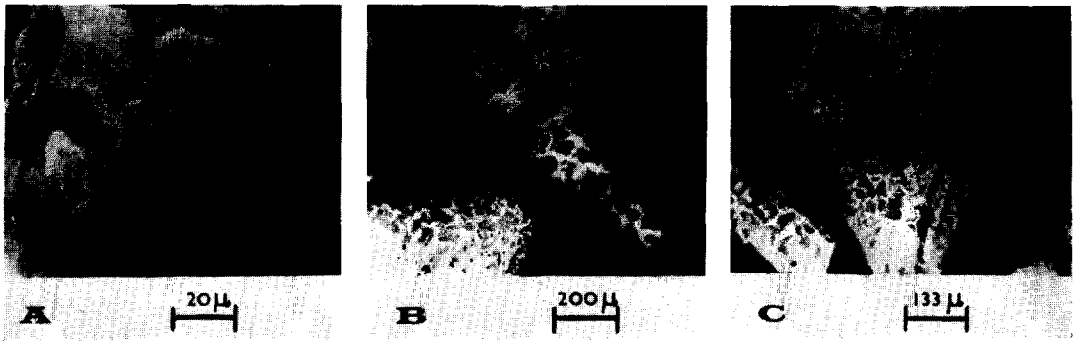

FIG. 3. (A and C) are optical micrographs of the 42 wt % nickel alloy B, containing β- and γ- eutectic phases. A micrograph of the 50 wt % nickel alloy A, containing only dark colored γ-phase grains in a matrix of the lighter colored β-phase, is given in (B).

2. The Reaction of Raney Alloys with Sodium Hydroxide

The reactivity of the polished alloy surface to sodium hydroxide has been studied (*5*). The order of reactivity found was:

$$\text{eutectic} > NiAl_3 > Ni_2Al_3.$$

We have repeated such experiments, etching 42/58 alloy with 20% aqueous NaOH at room temperature, since this material contains all three constituent phases. Under these conditions eutectic and β-phase react rapidly, while γ-phase apparently did not begin to react for 25 min at which time brown discoloration could be observed. The γ-phase was therefore much the least reactive and the removal of eutectic (95 wt % Al) to leave voids was rapid. We could not, however, distinguish between the rates of reaction of β phase and eutectic. For example, immersion for 1 min darkens β-phase sufficiently to reverse the contrast between β and γ, at which time the eutectic precipitate is apparently unreacted. After 4 min, many areas of β-phase begin to show surface pitting, again at a time when reaction of eutectic is small. Prolonged etching (15 min), not yet sufficient to cause reaction of γ, results in the appearance of microcracks

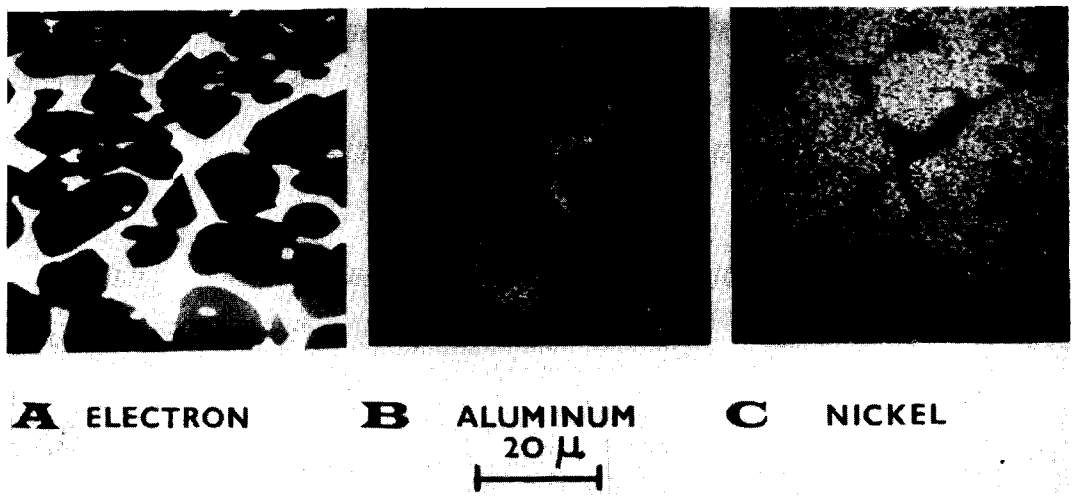

FIG. 4. Microprobe scans of an area of surface of alloy B which contained only the eutectic and β-phase. The eutectic precipitate, having a lower average atomic weight, reflects fewer electrons and consequently is light in color in records of specimen current (A). The higher aluminum content, and therefore nickel deficiency, of the eutectic is illustrated by the aluminum and nickel $K\alpha_1$ scans in (B and C).

FIG. 5. Optical micrographs of alloy A after reaction with concentrated aqueous sodium hydroxide. The interface between reacted and unreacted alloy in a cross-sectional sample (see text for details) is shown in (A), where the unreacted areas within the product zone were found to be γ-phase. Similar areas of unreacted γ-phase (lightest in color) are shown in more detail in (B). A typical micrograph of the structure observed after 10-min reaction of 30–50 mesh alloy A is given in (C); the white areas were unreacted γ-phase.

in the β-phase, concurrent with the formation of voids formerly occupied by eutectic. A similar broken structure of reacted β-phase is shown in the micrographs of Mason (*5*). We believe these microcracks were too irregular to be associated with subgrain structure and suggest that they are in fact shrinkage voids due to the volume contraction accompanying aluminum removal. In support of this conclusion, it may be noted that similar cracks were observed in reacted γ but were more prevalent in reacted β-phase which would be expected to undergo larger volume changes. The possibility that such phenomena are due to the etching of cold-working faults induced during polishing is considered unlikely, since similar features are encountered at appreciable depth in sectioned samples (see Fig. 5B) and in micrographs of the completely extracted catalyst (Fig. 6A and B).

The depth to which reaction of β-phase penetrates before attack occurs on γ-phase was then investigated by examining a polished section perpendicular to the original direction of caustic attack. The 50/50 alloy was used because of its low concentration of eutectic and larger γ grains. Polished alloy surfaces were reacted for various times in 20% NaOH at 50°C, washed in water and ethanol, capped with

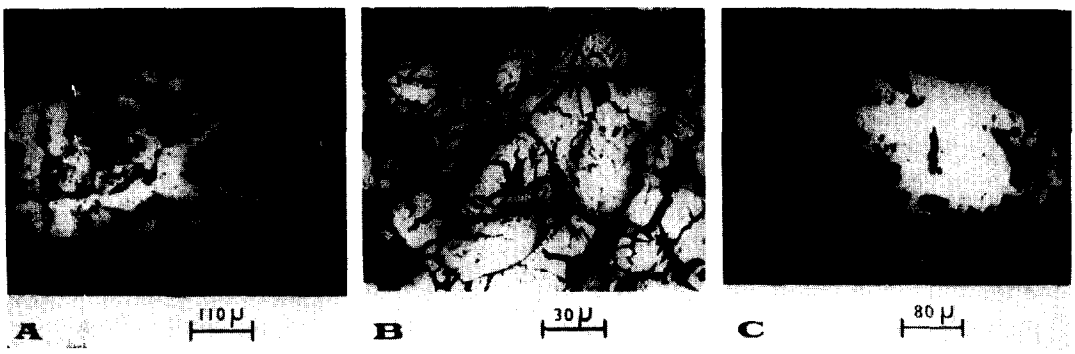

FIG. 6. The structures of 30–50 mesh pieces of 50 wt % nickel alloy A after prolonged extraction at 50 and 107°C in 20% aqueous NaOH are shown in (A and B), respectively. In (A), catalyst originating from the former γ-phase grains is lighter in color than that from β-phase, while the reverse is true in (B). The small white areas in (A) are unreacted γ-phase. The structure shown in (C) is typical of that found for samples extracted by the IGT method. No preferential reaction amongst the alloy phases is observed; partly reacted alloy pieces contain an unreacted core of all phases, surrounded by extracted catalyst.

mounting resin, sectioned perpendicular to the original surface plane, and the newly cut face was polished. In contrast to the lightly etched samples discussed above, penetration of several microns was required in order to examine the reaction interface, and the surface was pyrophoric. The reacted surface was therefore "capped" with cold mount just prior to complete solvent evaporation and the required cross-section was obtained on a coarse silicon carbide paper under water. Normal polishing procedures could then be followed.

Reacted and unreacted alloy could be distinguished, and the reaction of β proceeded to an average depth of some 60 μ before γ-phase began to react. Preferential reaction was still evident after much longer periods of reaction, the "product scale" containing unreacted γ-phase (Plate 3A). A higher magnification view of some of these partly reacted γ grains is given in Fig. 5B. The presence of an unreacted core surrounded by extracted catalyst may be seen in such grains.

Electron probe studies of these samples confirmed the conclusions based on optical appearance. For example, the bright, apparently unreacted regions in the product scale gave identical nickel and aluminum counting rates to those obtained from γ-phase. The darker, reacted regions gave data quantitatively similar to those obtained with completely extracted catalyst. It may also be noted, that to the scale of probe resolution, no variation in aluminum concentration could be observed on approaching the reaction interface from either the reacted (Raney nickel) or unreacted (β or γ alloy) sides.

It must be emphasized that a degree of subjective judgment is required in reaching these conclusions. The impact area of the electron beam is observed optically and the nature of the volume analyzed is assigned in this way. However, the element of volume analyzed is not always of the same structure as the area of surface thus viewed. Occasional contradictory data, statistically outweighed by "normal" readings, were therefore ascribed to regions where a different phase or a hole just beneath the surface had contributed to the analysis but was not visible optically.

Frequently, this assumption could be supported by other data. Holes, for example, could often be detected by probe scanning and oscilloscope display, giving lowered intensity in both nickel and aluminum $K\alpha_1$ relative to surrounding areas. Subsurface structures different from the visible probe impact area (e.g., a γ-phase grain perhaps 0.25 μ below an area identified optically as reacted β phase), are more difficult to prove, but may show up in displaying the specimen current variations from the region.

Assuming 30–50-mesh alloy pieces to be spheres of similar dimensions to the openings in a 30-mesh sieve (radius 0.03 cm) and that the reaction of such spheres with sodium hydroxide may be related to the planar etching reaction described above, the degree to which β-phase may react preferentially in a standard extraction process can be estimated. Such calculations suggest that all accessible β-phase in the powdered alloy will be converted to Raney nickel in about 10 min (compared to about 100 min for complete reaction), and that γ-phase will be little reacted in this period. To test this postulate 6 g of 30–50 mesh, 50/50 alloy were added to 200 ml of 20% NaOH at 50°C. The reaction was carried out in a well stirred glass reactor (7) and hydrogen evolution was measured by a wet-test meter. After 10 min extraction, polished samples of the partly reacted solid had a structure typified by that shown in Fig. 5C. Electron probe analysis showed that the bright areas were unreacted γ-phase, the darker, reacted regions, apparently Raney nickel. After 90-min reaction, most pieces contained no unreacted alloy. An occasional larger piece did contain a little unreacted γ-phase and micrograph 6A shows one such piece, in which the three small white areas were identified as Ni_2Al_3. The contrast between other areas in this micrograph is between reacted γ and reacted β, the former being somewhat lighter in color. This assignment was demonstrated more clearly by aluminum extraction from pieces of 42/58 ingot

in which the γ-phase had a markedly dendritic appearance. This "memory" of the grain structure of the original alloy was stable thermally, 24-hr evacuation at 450°C producing no visible change. The catalyst particles have low mechanical strength, however, slight stress being sufficient to grind the material.

The hydrogen evolved in a 10-min extraction corresponded to about 50% of complete reaction assuming the stoichiometric reaction:

$$2Al + 2NaOH + 2H_2O \rightarrow 2NaAlO_2 + 3H_2. \quad (1)$$

The rate of reaction, deceleratory throughout, decreased markedly after 10 min. The hydrogen evolved after 90 min was 90% of that required by Eq. (1). These values are consistent with the metallographic data.

Littman and Bliss (*4*) observed two distinct areas in optical micrographs of activated commercial Raney nickel, and suggested that the different areas may have been derived from different nickel–aluminum alloys. In their published micrographs (*4*), areas derived from the β-, and γ-phases can be identified; however, the contrast is the reverse of that shown in Figure 6A for a catalyst activated at 50°C. We have observed the same reversal of contrast for catalysts prepared under more severe conditions, e.g., Raney nickel prepared by reaction in boiling 20% alkali for 2 hr [cf. catalyst $IIIA_2$ in Part I (*7*)] shown in Fig. 6B.

Mason (*5*) found equal reactivities for the γ- and β-phases of Raney alloys to aqueous alkali; both metallographic and X-ray diffraction studies showed unreacted γ and β alloys coexistent in catalyst particles. However, these catalysts prepared at the Institute for Gas Technology (IGT) were activated with substantially less than the stoichiometric amount of NaOH required for Eq. (1). We have prepared catalysts by a similar method [Type IV catalysts of Part I (*7*)]. In one such preparation, 30 ml of 20% NaOH [about ¼ of the requirements of Eq. (1)] were added to 40 g of 50–100 mesh, 50/50 alloy in 300 ml of distilled water at 80°C. An initially rapid reaction soon subsided and was followed by a short induction period, after which rapid hydrogen evolution recommenced. Reaction was stopped when the evolved hydrogen corresponded to 80% of that predicted for complete aluminum oxidation. The solid was washed to neutrality in distilled water, large flocks of alumina being evident in the decanted layers. A typical micrograph of this material is given in Fig. 6C. Reacted and unreacted alloy may be clearly distinguished and both γ and β alloys are present in the unreacted core of the particle as demonstrated by Mason (*5*). Contrast between reacted γ and β, reported by Mason, is again observed, and it may be noted that such contrast is much more clearly defined in this type of preparation.

Quantitative Electron Probe Microanalysis

Electron probe microanalysis was used to examine two problems defined by the preceeding optical studies: (i) Did the retention of grain structure between alloy and catalyst and the optical contrast between catalyst derived from $NiAl_3$ and from Ni_2Al_3 correspond to a difference in chemical composition? (ii) To the spatial resolution of microprobe analysis, perhaps 1 μ^3 under favorable circumstances, were areas of similar optical appearance also areas of the same chemical composition?

Experimental data were obtained largely at 25 kV beam voltage 50 nA specimen current. Since operating voltage is normally chosen to be about three times the critical excitation voltage for the element and X-ray line desired, the operating voltage was optimized for nickel analyses for the most part. For materials of low aluminum content, aluminum $K\alpha_1$ intensities were very small under these conditions (Fig. 1) and aluminum analyses consequently of lower accuracy. Additional data were obtained at 11.5 kV, 20 nA for such catalysts. Aluminum $K\alpha_1$ intensities were then appreciably larger relative to pure aluminum and more accurate calibrations could be obtained at low aluminum concentration.

Standard counting techniques were used to examine several catalyst preparations in detail. Six particles of each preparation were studied and about 30 point counts

TABLE 3
MICROPROBE ANALYSES FOR A VARIETY OF RANEY CATALYSTS

Catalyst type	Regions analyzed	25 kV Ni (%)	25 kV Al (%)	11.5 kV Ni (%)	11.5 kV Al (%)	Chemical analysis Ni (wt %)	Chemical analysis Al (wt %)
1. Prepared at 50°C [types IA, IIA, and IIB of Ref. (7)]	γ-derived	79	10	78	6	81	8.2
	β-derived	79	6	76	3		
2. Data from interface of etched (50/50) alloy of sectioned type	γ-derived	82	10				
	β-derived	82	5				
3. Prepared at 107°C [type IIIA of Ref. (7)]	γ-derived	82	3	84	2.5	86	5.2
	β-derived	86	1.5	88	1		
4. IGT Type from 50/50 alloy [type IV of Ref. (7)]	γ-derived	59	16			49	22
	β-derived	44	17				

were taken from different regions of each particle. For each point count, sufficient data were obtained to ensure reasonable statistical accuracy. Nickel and aluminum X-ray intensities were first expressed as a fraction of the intensities for pure nickel and aluminum and then corrected using the calibration curve of Fig. 1, or the corresponding calibration at 11.5 kV. All results for any particular catalyst were then averaged over the region analyzed, i.e., area that had originated from γ or β alloy. Data of this type, together with the relevant nickel and total aluminum analyses obtained by chemical methods are given in Table 3. Details of the results obtained may be summarized thus:

(i) For any given catalyst of types I, II, and III (7), nickel intensities were relatively constant (±5%) from one point to another in either the regions derived from β alloy or those derived from γ alloy. Similar data for different catalysts prepared in the same way was only slightly less reproducible (mean deviation ±7%), and all catalysts of types I and II gave equivalent results within these limits. Data were less reproducible (±15%) for the type IV (IGT) catalyst and only in this case was significant variation in nickel content between the γ- and β-derived regions noted.

(ii) In general, aluminum analyses showed greater variation (mean deviation ±20%) in optically similar regions. For all except the type IV catalyst, however, the average of such values from one particle to the next was always relatively reproducible (±5%) and marked variation in the aluminum content of the two catalyst regions was always observed (Table III). Averaged values for the type IV catalyst were also reproducible to ±5%, but no systematic variation between aluminum analyses for β- and γ-derived regions of the catalyst was observed.

To the scale of probe resolution, therefore, the chemical composition of types I, II, and III catalysts appears to be homogeneous in optically similar regions. However, those regions of catalyst formed from the Ni_2Al_3 grains of the original alloy contain approximately twice as much aluminum and/or alumina as regions formed from $NiAl_3$. This is not observed in the type IV catalyst. However, the large quantities of alumina trihydrate present in this catalyst, apparently unevenly distributed, may mask a similar difference in the amount of aluminum yet unreacted. Both nickel and aluminum analyses were in acceptable agreement with the chemical data, even in the case of the type IV catalyst, estimated (7) to contain about 42 wt % β $Al_2O_3 \cdot 3H_2O$.

The present data therefore suggest that

standard electron probe techniques yield analyses of moderate accuracy when applied to microporous materials. This result may best be understood by considering the characteristic X-radiation obtained from any nonporous solid and from the same solid in microporous form such that pore size is very small compared to probe resolution. In neither case will the whole of the incident electron flux generate X-rays. A certain fraction, determined largely by atomic number and surface topography, will be back-scattered with little loss of energy, but this quantity would not be expected to vary significantly between the porous and nonporous case. For the nonporous solid, the volume in which characteristic X-radiation is generated may be represented by the shaded area of Fig. 2. Schematically, an electron may be considered to penetrate to a depth SA and emerging X-ray quanta must pass through a distance AB in the solid en route to the spectrometer. For the microporous element, the volume analyzed (broken line) will be larger, the same electron may penetrate to a depth SA′ and the emerging X-ray quanta must pass through a distance A′B′ in the specimen.

However, to a first approximation, the volume analyzed will contain the same mass in either case. Thus an electron moving between S and A will encounter the same weight of solid as that moving along S′A′ and will generate the same amount of X-radiation. Further, since all distances within the specimen are small relative to the distance between specimen and spectrometer, AB and A′B′ will be approximately parallel and emergent X-ray quanta will also encounter equivalent mass and undergo similar absorption processes. These relationships are shown by equations for electron penetration and X-ray emission and for X-ray absorption, which are functions only of mass–distance (*12*).

Clearly, these arguments would not be true for a material containing pores of a size similar to probe resolution. It may be noted, however, that mean pore diameters for the nickel catalysts used in the present work were about 30–60 Å (*7*).

Discussion

Samples of commercial 42 and 50 wt % nickel alloys were found to contain the same three phases; Ni_2Al_3, $NiAl_3$, and a eutectic precipitate. NiAl was not detected in this batch of 50/50 alloy, although it has been observed (*5*) in other alloys of this composition. The 50/50 alloy contained a little more Ni_2Al_3 and substantially less eutectic phase than the 42/58 material.

One cannot assume similar structural differences between all 42/58 and 50/50 alloys. It is clear from the phase diagram (*3*) that the method of cooling will greatly influence the microstructure. However, it seems reasonable to conclude that the differences observed would be predicted from the phase diagram for quenched alloys and might be anticipated on a more general basis for alloys prepared by rapid cooling of a well-mixed melt.

The fundamental difference in microstructure of the two alloys studied was the appearance of much of the additional aluminum content of the 42/58 material as eutectic precipitate. This eutectic phase, for which an average nickel content of about 5 wt % has been confirmed, must not be expected to contribute significantly to the final nickel catalyst. Thus, during reaction with sodium hydroxide, regions of eutectic precipitate were largely dissolved to leave voids in the alloy particles. In contrast, the residue after aluminum removal from both $NiAl_3$ and Ni_2Al_3 retained much of the appearance of the starting alloy since optical contrast between distinctive areas of the polished catalyst could be related to the original $NiAl_3/Ni_2Al_3$ grain structure. Electron microprobe analyses further showed that Raney catalyst originating from Ni_2Al_3 contained about twice as much aluminum and/or alumina as that originating from $NiAl_3$. This was true of catalysts prepared at 50°C (Fig. 6A) and also of those prepared in boiling alkali (Fig. 6B) when the previous optical contrast between γ-derived and β-derived catalyst was reversed and the overall aluminum content was lower due to the more severe reaction conditions.

Optical examination of cross-sections of the reaction interface suggests that the removal of aluminum from both $NiAl_3$ and Ni_2Al_3 is an "advancing interface" type process and not a reaction proceeding via intermediate compounds or the progressive removal of aluminum over the whole particle. Electron probe microanalysis shows the absence of gradients of aluminum concentration at the reaction interface and equivalent aluminum concentrations in the reacted zone of partly extracted alloy to those in the final catalyst. The data of Sassoulas and Trambouze (*2*), who found that Ni_2Al_3 and nickel were the only crystalline phases detectable in partially extracted Ni_2Al_3, is consistent with such a process.

Sassoulas and Trambouze (*2*) also report that pure $NiAl_3$ reacts more readily with aqueous sodium hydroxide than pure Ni_2Al_3. This is found to be equally true of these phases in the present multicomponent alloys. Thus, when reaction was carried out in an excess of concentrated alkali in the normal way, markedly preferential reaction of $NiAl_3$ was observed (Fig. 5). Literature data involving partly extracted catalyst must therefore be interpreted with care; for example, the hydrogen evolved may not be a good measure of the fraction of the nickel that has been activated.

The nonselective reaction, reported by Mason (*5*) and thought to signify a difference in behavior between the pure phases and the multiphase alloy, has been shown to result from a different method of catalyst preparation in which the amount of sodium hydroxide does not satisfy the stoichiometric requirements of Eq. (1). Dirksen and Linden (*9*) suggested two possible contributory reactions in addition to Eq. (1):

$$2Al + 6H_2O \rightarrow Al_2O_3 \cdot 3H_2O + 3H_2, \quad (2)$$

$$2NaAlO_2 + 4H_2O \rightarrow Al_2O_3 \cdot 3H_2O + 2NaOH. \quad (3)$$

Equation (1) appears to offer an adequate description of the standard activation process. The hydrolysis of sodium aluminate [Eq. (3)] during subsequent water washing may well yield much of the β $Al_2O_3 \cdot 3H_2O$ known (*10*) to exist in the final catalyst. The IGT activation process may well involve a combination of (1) and (3), the necessary alkali ions being continually regenerated by the hydrolysis reaction to yield the high alumina content of these catalysts reported by Dirksen and Linden (*9*) and confirmed in the present study. The IGT and the normal activation processes lead to similar products with small nickel crystallites (*5*), comparable porosity (*7*) and catalytic activity (*11*). Apparently, the low alkali concentration in the former method is reflected only in the large amounts of hydrated alumina present. The equivalent rates of reaction of $NiAl_3$ and Ni_2Al_3 in the IGT activation is presumably caused by a change in rate-determining step between the two extraction methods.

Acknowledgments

The authors are grateful to the Davison Chemical Co. Ltd., for fellowship funds, to Dr. F. G. Ciapetta and N. E. Miller for catalyst samples and helpful discussions, to Professor G. R. Purdy and H. W. Walker, for guidance in the interpretation of results and the operation of the electron probe microanalyzer of the Metallurgy and Material Science Department, and to the National Research Council for providing the electron probe.

References

1. Lieber, E., and Morritz, F. L., *Advan. Catalysis* **5**, 417 (1953).
2. Sassoulas, R., and Trambouze, Y., *Bull. Soc. Chim. France* **5**, 985 (1964).
3. Alexander, W. O., and Vaughan, W. B., *J. Inst. Metals* **61**, 247 (1937).
4. Littman, H., and Bliss, H., *Ind. Eng. Chem.* **51**, 662 (1959).
5. Mason, D. McA., in Ref. (*9*).
6. Kabiev, T., Fasman, A. B., Isabekov, A., and Chernousova, K. T., *Elektrokhimiya* **1**, 868 (1965).
7. Freel, J., Pieters, W. J. M., and Anderson, R. B., *J. Catalysis* **14**, 247 (1969).
8. Rostoker, W., and Dvorak, J. R., "Interpretation of Metallographic Structures," Chap. 5. Academic Press, New York, 1965.
9. Dirksen, H. A., and Linden, H. R., *Inst. Gas Technol. Res. Bull.* **31**, (1963), 137.
10. Kokes, R. J., and Emmett, P. H., *J. Am. Chem. Soc.* **81**, 5032 (1959).

11. FREEL, J., ROBERTSON, S. D., AND ANDERSON, R. B., *J. Catalysis,* submitted for publication.

12. CASTAING, R., *in* "Third International Symposium on X-Ray Optics and X-Ray Microanalysis" (H. H. Pattee, V. E. Cosslett, and A. Engstrom, eds.), p. 263. Academic Press, New York, 1963.